Highlights on Spanish Astrophysics X, Proceedings of the XIII Scientific Meeting of the Spanish Astronomical Society held on July 16 – 20, 2018, in Salamanca, Spain. B. Montesinos, A. Asensio Ramos, F. Buitrago, R. Schödel, E. Villaver, S. Pérez-Hoyos, I. Ordóñez-Etxeberria (eds.), 2019

Multi-wavelength mock observations (of the WHIM) in a simulated galaxy cluster.

Susana Planelles[1], Petar Mimica[1], Vicent Quilis[1,2] and Carlos Cuesta-Martínez[1]

[1] Departament d'Astronomia i Astrofísica, Universitat de València, c/ Dr. Moliner, 50, 46100 - Burjassot (València), Spain
[2] Observatori Astronòmic, Universitat de València, E-46980 Paterna (València), Spain

Abstract

In this contribution we introduce a novel numerical approach, based on a full-radiative transfer code, which is able to generate multi-wavelength synthetic observations of the gas component in cosmological simulations by integrating the transfer equation along the null-geodesic of photons. In order to test the capabilities of this numerical tool, we have applied the code on a large galaxy cluster developed in a full cosmological simulation and we have compared the emission associated to the whole inter-galactic medium (IGM) and to the warm-hot intergalactic medium (WHIM) gas components in three different energy bands: in soft X-rays, through the thermal Sunyaev-Zel'dovich (SZ) effect and in radio.

1 Introduction

As suggested by hydrodynamical simulations [10], most of the "missing" baryons are supposed to be located in a mildly overdense, warm-hot intergalactic medium (WHIM). The WHIM, which is thought to contain ∼50% of the local cosmic baryons, is expected to be mainly in filaments but also around large clusters and between pairs of interacting systems. Therefore, the WHIM plays a central role in the solution of the "missing baryons problem". Moreover, despite its relatively low densities (from $\sim 4\times10^{-6}$ to $\sim 10^{-4}$ cm^{-3}) and temperatures ($10^7 - 10^8$ K), the WHIM also represents a perfect scenario for multi-wavelength observations. In this sense, the forthcoming generation of telescopes will certainly improve our understanding of the WHIM in several wavelength bands.

Within this context, our goal is to use a well-resolved simulated galaxy cluster to generate multi-wavelength synthetic images (of the IGM and of the WHIM) directly comparable with observations. In order to compute the emission, we introduce a novel numerical approach, based on a relativistic full-radiative transfer code, to post-process the simulation data. To compute the change in the intensity along each line of sight, the code integrates the

null-geodesic of photons. Although in our case the absorption is negligible, the code is also able to compute the self-absorption. Therefore, in this contribution we briefly compare the emission associated to the IGM and to the WHIM gas components in soft X-rays, through the thermal SZ (tSZ) effect, and in radio at a frequency of 1.4 GHz. We wish to emphasize that all bands are treated consistently, without tuning of parameters, by the same code.

While this is just a short contribution, we refer the interested readers to [11], where an extended and more detailed description of the employed numerical approach and of the obtained results is presented.

2 Numerical details

Below we only provide a brief description of the present study, while we refer the reader to [11] for further details.

2.1 The cosmological simulation

We analyse a simulation performed with the cosmological code MASCLET [12]. The simulation, which accounts for a flat ΛCDM universe, consists in a computational box with a comoving side length of 40 Mpc, with a peak physical spatial resolution of ~ 610 pc at $z = 0$ (see [13] for further details). The best mass resolution for the dark matter particles is $\sim 2 \times 10^6\, M_\odot$. The simulation is set up to develop a big galaxy cluster at the centre of the computational domain.

Besides gravity and hydrodynamics, the simulation includes inverse Compton and free-free cooling, UV heating, atomic and molecular cooling for a primordial gas, cooling rates dependent on metallicity, star formation and feedback from SN-II. However, feedback from SN-Ia, stellar winds, or AGN are not included.

Using the halo finder ASOHF ([8, 4]) we have identified the central and largest halo ($M_{vir} \sim 3.2 \times 10^{14} M_\odot$ and $R_{vir} \sim 1.7$ Mpc) in the simulation at $z = 0.33$. In the following, we will analyse the X-ray, SZ or radio signals coming from inside and from an extended region of $5 \times R_{vir}$ around this main central halo. Within this region we will consider two gas components: the IGM (formed by all the gas elements) and the WHIM (formed by those gas elements with a temperature within $10^5 K < T < 10^7 K$).

2.2 Computing the emission

To compute the thermal and non-thermal emission in different observational bands we employ the full-radiative transfer code SPEV [6, 7, 1]. SPEV can produce consistent multi-band and multi-epoch synthetic observations by following the emission along the null-geodesics. Therefore, in order compute the emission from MASCLET outputs, we apply SPEV in post-processing (see [11] for further details on the code). In particular, we have implemented in SPEV the computation of three different signals:

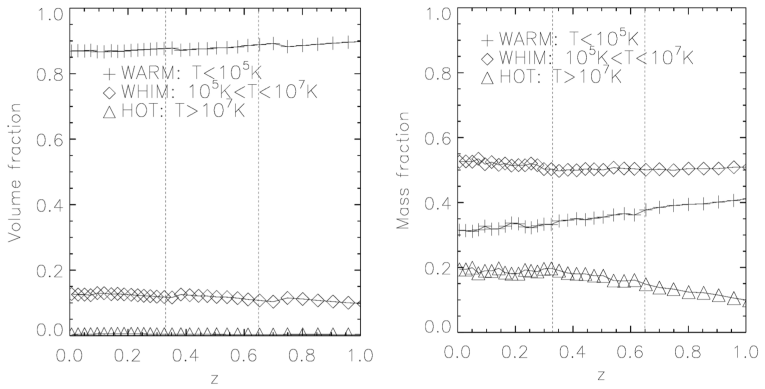

Figure 1: Evolution with redshift of the fraction in volume (left) and in mass (right) occupied by different gas components within the whole simulated domain. Figure from [11].

- Thermal emission. In order to account for the contribution from both free-free thermal Bremsstrahlung and metal line emission, we built a large interpolation table of the X-ray emission in different energy bands using the publicly available code CLOUDY [3].
- Non-thermal emission. To compute the synchrotron emission at different frequencies, we accounted for several simplifications: we assumed that the magnetic field satisfies flux conservation, we did not include any transport scheme for the non-thermal (NT) electrons, and we used a simplified formalism to estimate the NT electron distribution.
- The SZ effect. We took advantage of the way in which SPEV sorts the data along different lines of sight to compute the thermal (tSZ) and kinematic (kSZ) SZ effects in the non-relativistic approximation.

3 Results

As a consistency check, Fig. 1 shows the redshift evolution of the fractions in mass and in volume occupied by the warm ($T < 10^5 K$), the WHIM ($10^5 K < T < 10^7 K$), and the hot ($T > 10^7 K$) gas components within the whole simulated box. As expected, most of the volume is occupied by the warm and the WHIM gas components. In agreement with previous studies, the WHIM represents up to $\sim 55\%$ of the mass content at $z = 0$.

Figure 2 shows the density maps, projected along the line of sight, of the IGM and of the WHIM gas phases within our volume of interest. As expected, while the central cluster dominates the IGM map, in the case of the WHIM the map is mainly connected to the smallest objects and shows a much more filamentary and volume-filling distribution.

In Fig. 3 we show a sample of some of the mock images we presented in [11]. In particular, we show, for IGM and WHIM (top and bottom rows, respectively), the soft X-ray emission (left column), the signal associated to the tSZ effect at $\nu = 128$ GHz (middle

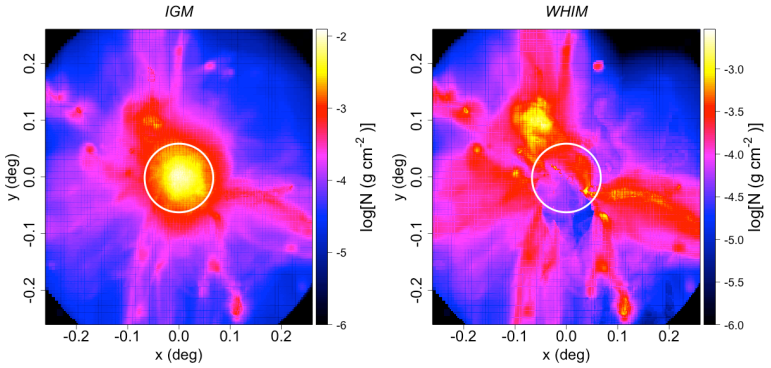

Figure 2: Surface density maps of the IGM and the WHIM gas components within a region of $\sim 0.6^\circ \times 0.6^\circ$ around the main cluster in the simulation. The cluster virial radius is represented by the white circle. Figure from [11].

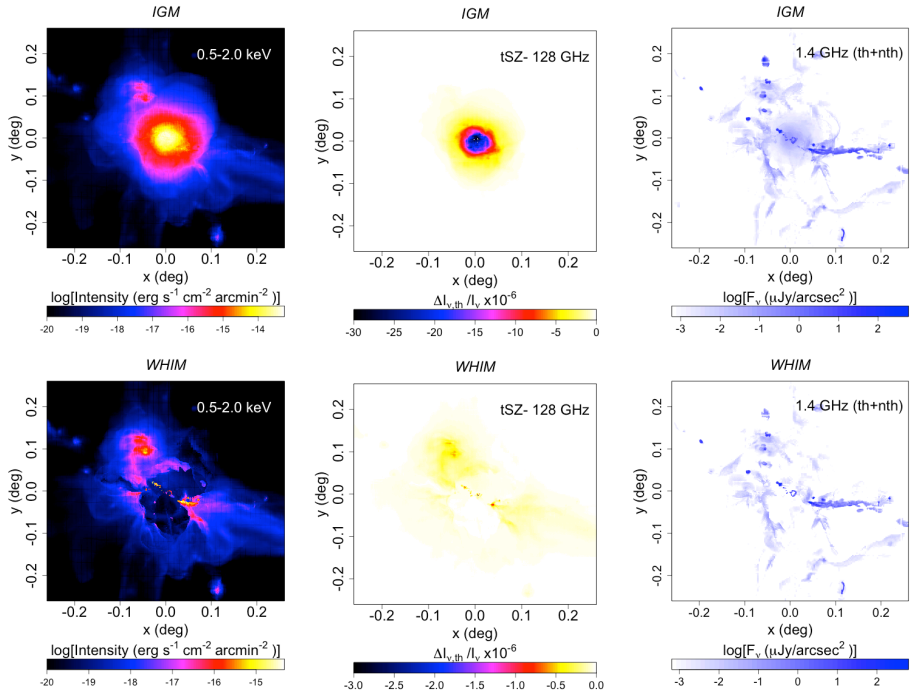

Figure 3: *Left column:* X-ray thermal emission maps associated to the IGM and to the WHIM gas components (top and bottom rows, respectively) at the soft $(0.5 - 2$ keV) energy band. *Middle column:* Intensity maps, $\Delta I/I_\nu$, of the thermal SZ effect at $\nu = 128$ GHz for the IGM and the WHIM. *Right column:* Mock radio observations of the IGM and the WHIM gas components at 1.4 GHz for a beam size of 1×1 arcsec^2. Composited image from [11].

column), and the radio emission at 1.4 GHz (right column).

The synthetic X-ray emission maps shown in the left column of Fig. 3 have a pixel size of $\sim 0.68''$. Although this resolution is in line with that of *XMM-Newton* and *Chandra*, we did not account for the response function of any specific observational instrument. Qualitatively, as already shown in previous studies, most of the IGM thermal emission is detected in the soft regime, where the emission from small structures is highlighted. Instead, the WHIM emission is mainly found in outer cluster regions around the main cluster with a more filamentary and extended distribution. Quantitatively, we obtain a broad agreement between the IGM soft X-ray emission associated to our simulated cluster and recent observations of massive galaxy clusters (e.g. [2]).

As shown in the middle column of Fig. 3, the tSZ signal at $\nu = 128$ GHz shows always negative values and is dominated by the main galaxy cluster, which can reach central intensities as high as $|\Delta I_{\nu,th}/I_{\nu}| \sim 3 \times 10^{-5}$. Regarding the WHIM, most part of the central tSZ signal is removed, leaving a much fainter and outer distribution around the cluster. On average, most part of the tSZ signal is contributed by hot and/or massive structures. Despite the weakness of the WHIM tSZ effect, its observational detection, especially at high redshift, represents a valuable complementary approach to X-ray observations.

Analyzing the radio maps shown in the right column of Fig. 3, we can draw several general conclusions: (i) only a small fraction of the cluster volume emits in radio, (ii) the IGM radio emission is correlated with dense and hot IGM regions and, (iii) there is a minor radio signal at the very outer cluster regions ($r \geq 4 \times R_{vir}$). Overall, IGM and WHIM have a maximum radio signal of around half mJy arcmin^{-2} at 1.4 GHz. In our case, the comparison of these radio maps with the distribution of shock waves (see [9, 5] for details on the detection of shocks) suggests that most of the cluster radio emission is connected to weak internal shocks within the cluster, whereas there is only a tiny contribution from strong external accretion shocks.

4 Summary and conclusions

In view of the next generation of improved observational facilities (e.g. *ATHENA+*, *SKA* or *CCAT-prime*), it is important to produce and analyse proper multi-band synthetic observations derived from full cosmological simulations. The combination of observational and synthetic images of the cosmic web in different bands is crucial to deepen our knowledge of the IGM physics in a number of aspects.

In this short contribution (an extended analysis is presented in [11]), we analyse a massive galaxy cluster, formed in a full cosmological simulation, through the comparison of the spatial distributions and the emissions associated to the IGM and to the WHIM gas components in different wavebands. In order to generate proper synthetic observations of the IGM and of the WHIM gas components, we present a novel numerical approach, based on the full-radiative transfer code SPEV [6], that integrates the transfer equation along the null-geodesic of photons in order to compute the intensity along each line of sight. We have modified SPEV in order to estimate, using exactly the same numerical scheme, the emission

in X-rays, through the thermal SZ effect, and in radio at different frequencies. In general, as discussed in [11], we obtain at all three bands a broad agreement with previous numerical and observational estimates.

We would like to emphasize that this analysis represents our first attempt in the design of a complex numerical approach able to treat, consistently, the IGM emission at any observational frequency. Despite the optimistic results we have obtained, the employed simulation and the presented numerical procedure show some limitations that we will certainly improve in the near future. In this regard, now that the method has been tested, we are working on a new set of larger and improved simulations (in terms of physics and statistics) that will produce a larger sample of clusters. Moreover, we are already improving the estimation of the different observational signals in SPEV in order to produce improved and more realistic mock observations.

Acknowledgments

We acknowledge support by the *Spanish Ministerio de Economía y Competitividad* (MINECO, grant AYA2016-77237-C3-3-P). SP is "Juan de la Cierva" fellow (ref. IJCI-2015-26656) of the Spanish MINECO. PM acknowledges the support from the European Research Council (grant CAMAP-259276). CC-M acknowledges the support of ACIF/2013/278 fellowship.

References

[1] Cuesta-Martínez, C., Aloy, M. A. & Mimica, P. 2015, MNRAS, 446, 1716

[2] Eckert, D. et al. 2015, Nature, 528, 105

[3] Ferland, G. J. et al. 2017, MNRAS, 53, 385

[4] Knebe, A. et al. 2011, MNRAS, 415, 2293

[5] Martin-Alvarez, S., Planelles, S. & Quilis, V. 2017, ApSS, 362, 91

[6] Mimica, P. et al. 2009, ApJ, 696, 1142

[7] Mimica, P. et al. 2016, Journal of Physics Conference Series, 719, 012008

[8] Planelles, S. & Quilis, V. 2010, A&A, 519, A94

[9] Planelles, S., Quilis, V., 2013, MNRAS, 428, 1643

[10] Planelles, S., Schleicher, D. R. G. & Bykov, A. M. 2015, SSR, 188, 93

[11] Planelles, S., Mimica, P., Quilis, V. & Cuesta-Martínez, C. 2018, MNRAS, 476, 4629

[12] Quilis, V. 2004, MNRAS, 352, 1426

[13] Quilis, V., Planelles, S. & Ricciardelli, E. 2017, MNRAS, 369, 80